RSC Advances

PAPER

View Article Online
View Journal | View Issue

Cite this: *RSC Adv.*, 2025, **15**, 14745

Numerical analysis of the impact of non-uniform gas diffusion layer deformation on the performance of proton exchange membrane fuel cells

Wang Zheng, Yuzhen Xia, Hangwei Lei, Haoze Wang and Guilin Hu *

Proton exchange membrane fuel cells (PEMFCs) typically require assembly under specific conditions to ensure good air-tightness, mass transfer, and electrical conductivity. However, the stress and strain produced on cell components due to assembly pressure can affect the performance and lifespan of the cells. To thoroughly investigate the effects of assembly mechanics on the transport processes and output performance of the cells, this study employed the finite element method (FEM) through the ANSYS static structural module to analyze the deformation of the gas diffusion layer (GDL) and its material property changes under pressures ranging from 0.0 to 2.5 MPa. The adjustment of material properties following non-uniform deformation of the GDL was implemented using UDFs (User-Defined Functions) in FLUENT. A three-dimensional two-phase flow computational fluid dynamics (CFD) model of the PEMFC was established, and the transport processes and output performance of a single PEMFC under different assembly pressures were simulated based on the variable material properties UDFs. The results indicate that the optimal assembly pressure for the PEMFC lies between 1.0 and 2.0 MPa. At low voltages of 0.3 to 0.4 V, the cell exhibits better performance under assembly pressures of 1.0 to 1.5 MPa; at voltages of 0.5 to 0.7 V, better performance is achieved under pressures of 1.0 to 2.0 MPa. Finally, the impacts of different operating temperatures, gas relative humidity levels, and gas stoichiometric ratios on the cell performance for an optimal pressure of 1.5 MPa were analyzed. The results show that the cell performs best at a temperature of 353.15 K, with an anode relative humidity of 80% and a cathode relative humidity of 100%, and with an anode stoichiometric ratio of 2 and a cathode stoichiometric ratio of 3. These findings provide a theoretical basis for the assembly and high-performance operation of fuel cells.

Received 11th March 2025
Accepted 12th April 2025

DOI: 10.1039/d5ra01753j

rsc.li/rsc-advances

1. Introduction

PEMFCs using hydrogen and oxygen as electrochemical reactants are widely applied due to the advantages, including high energy efficiency, rapid startup, and zero emission.[1] The fuel cell components are assembled to avoid reactant gas leakage and maintain good contact and charge transfer. Under a certain assembly pressure, the electrode, typically made from porous carbon-based materials such as carbon paper, inevitably undergoes non-uniform deformation because of the channels and ribs.[2,3] Previous studies mainly focus on the gas diffusion layer (GDL), including the impact of assembly pressure and deformation on its microstructure, mechanical properties, and mass transfer characteristics, as well as the effect on water and heat transportation of the fuel cells.

The deformation degree of GDL is related to the value of assembly pressure.[4,5] Chen *et al.*[6] found that lower assembly pressure resulted in lower mass transport overpotential and higher ohmic overpotential. As GDL was over-compressed, both gas transportation and water drainage capabilities significantly decreased, indicating the great increase of mass transport polarization. Wang *et al.*[7] found that, in the region of assembly pressure below 1 MPa, the contact resistance decreased sharply with increasing pressure. Above 1.0 MPa, the effect is slight.

As the assembly pressure increases, the compression of GDL, particularly in the rib region, becomes more pronounced, resulting in increased electrical conductivity, reduced thickness and porosity.[8–10] Comparatively, GDL under the flow channels maintains a high stability because it is not directly compressed. The non-uniform between the two regions forms a gradient, which will change the electron pass path and mass transfer. Yan *et al.*[11] found that the non-uniform deformation produces a strong convection flux at the direction from GDL to flow channel, which is helpful for the liquid water drainage from GDL. The research results also indicated that water drainage from PEMFC stack by gas sweeping occupies a more important position than capillary effect. Therefore, the inhomogeneous deformation can enhance water management. Yang *et al.*[12] indicated that the effect of assembly pressure was different in the regions of GDL under the

School of Mechanical and Energy Engineering, Zhejiang University of Science and Technology, Hangzhou, China. E-mail: enehgl@163.com

rib and channel. It was reported that there is big differences in GDL porosity and GDL permeability near the rib/channel connection area causing more inhomogeneous transportation and distribution of reactants.[13–15] In addition, non-uniform deformation can also lead to uneven contact resistance distribution, which further affects the current density distribution and thermal management characteristics of PEMFC.[16–18]

Due to the complex and coupled transportation phenomena happing inside the fuel cell, CFD is pretty important and sometimes unique method to obtain distributions of physical parameters such as temperature species concentration.[19] The physical model is often simplified in the simulation of PEMFC research for the non-uniform deformation in the GDL. Chi *et al.*[20] assumed that GDL were uniform under the flow channels and ribs, using the average physical parameters in their simulation. Chippar *et al.*[21] combined FEM and CFD methods to numerically study the effects of GDL compression/intrusion on high-temperature PEMFCs using polybenzimidazole. The results showed that the compression and intrusion of inhomogeneous GDL had a significant impact on the transport performance of PEMFC. Su *et al.*[22] proposed a non-uniformly deformed GDL model, but did not consider the deformation at the junction of the channel and the rib. Zhang *et al.*[23] developed a comprehensive two-phase flow model coupling solid mechanics, heat and mass transfer, and electrochemical reactions. The results indicated that the distribution of ribs and channels caused significant deformation of the GDL and channel intrusion. Jiao *et al.*[24] established a gas–liquid–solid coupling model to study water and thermal management in PEMFCs after compression. Their research found that for the entire heat transfer process, the primary pathway for heat conduction was through the solid fiber layers in both dry and wet GDLs, while the concurrent water transport was also crucial in the wet GDL. Dong *et al.*[25] used a coupled FEM and CFD model to investigate the structural deformation and performance of PEMFCs at different membrane water contents. The study revealed that membrane deformation increased with higher water content, with greater expansion occurring beneath the flow channels compared to beneath the ribs. In the low current density range, the structural changes induced by membrane water content had a minimal impact on PEMFC performance; however, this influence became significant in the medium and high current density ranges.

In summary, assembly pressure significantly affects the internal transport processes and overall performance of fuel cells. Currently, there are much different kind of problems about the research on effects of assembly pressure on the transportation phenomena and cell performance. Some studies focus on the mechanical properties of PEMFCs, exploring the force distribution among components, but do not delve into the performance of the cells under actual operating conditions. Moreover, most studies are limited to single-channel PEMFCs, and the experimental conclusions drawn from single channels are difficult to fully reflect the complex situations of single cells, especially the internal transport characteristics. Additionally, many studies only consider single-phase fluids, overlooking the critical factor of water generation within the cell during operation. In light of this, this research builds upon the foundation of single-channel and single-phase flow fuel cell studies[26] and specifically investigates the issue of uneven deformation in the GDL for individual cells, proposing a new method to obtain the physical parameters of the uneven GDL. At the same time, a two-phase flow model is introduced into the PEMFC simulation, making the model more aligned with real operating conditions. This study not only identifies the optimal assembly pressure but also comprehensively analyzes the internal transport mechanisms of the cell. Lastly, the effect of operating temperature, gas relative humidity and stoichiometric ratio under optimal deformation conditions were further optimized after compression.

2. Mathematical model of the compression process

2.1 Geometric model

The schematic diagram of the PEMFC model is shown in Fig. 1. The overall model is a rectangular solid with dimensions 50 mm × 50 mm × 3.63 mm. The components of the model include a PEM with a thickness of 0.05 mm, a CL thickness of 0.01 mm, a GDL thickness of 0.28 mm, and a BP thickness of 1.5 mm. The flow channels have a height and width of 1 mm each, and the width of the ribs is also 1 mm (Table 1).

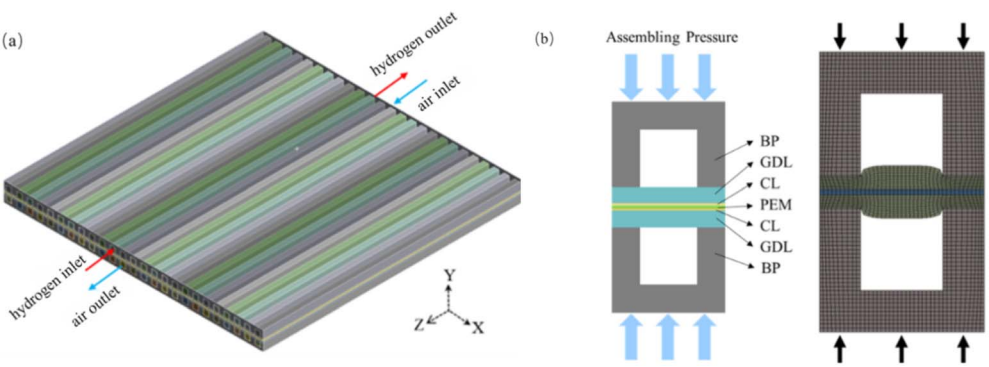

Fig. 1 PEMFC model: (a) single cell model; (b) main components of the PEMFC and schematic of compression deformation with girds.

Table 1 Basic parameters of the model

Parameter	Value
Channel width/height (mm)	1/1
Rib width (mm)	0.5
Electrode plate width/length/height (mm)	50/50/1.5
Initial GDL thickness[27] (mm)	0.28
PEM thickness (mm)	0.05
CL thickness (mm)	0.01
Initial contact resistance[27] (mΩ cm^2)	14.3

Table 2 Parameters of PEMFC components

Parameter	PEM	GDL	CL	Electrode plate
Density (kg m^{-3})	1980	1000	1000	1000
Young's modulus (MPa)	232	6.3	249	13 000
Poisson's ratio	0.253	0.256	0.3	0.26
Initial porosity	0.4	0.78	0.3	0
Conductivity[28] (S m^{-1})	9.825	300	300	20 000

2.2 Stress–strain equations

To deeply explore the solid mechanics performance of a three-dimensional PEMFC, particularly focusing on stress distribution and the deformation characteristics of the GDL, an analytical approach that integrates statics, geometry, and physics is employed. The quantitative relationships between strain and displacement, as well as between strain and stress, are described as follows.

The equation of force equilibrium:

$$\begin{cases} F_x + \dfrac{\partial \sigma_x}{\partial x} + \dfrac{\partial \tau_{yx}}{\partial y} + \dfrac{\partial \tau_{zx}}{\partial z} = 0 \\ F_y + \dfrac{\partial \sigma_y}{\partial y} + \dfrac{\partial \tau_{zy}}{\partial z} + \dfrac{\partial \tau_{xy}}{\partial x} = 0 \\ F_z + \dfrac{\partial \sigma_z}{\partial z} + \dfrac{\partial \tau_{xz}}{\partial x} + \dfrac{\partial \tau_{yz}}{\partial y} = 0 \end{cases} \quad (1)$$

where F_x, F_y and F_z represent the volumetric forces in the x, y and z directions, respectively; σ_x, σ_y and σ_z are the corresponding normal stresses; and τ_{xy}, τ_{yz} and τ_{zx} are the shear stresses on the xy, yz and zx planes, respectively. The shear stresses on different planes obey the principle of equal shear stress.

Distorted geometric equations:

$$\begin{cases} \psi_x = \dfrac{\partial u}{\partial x}, \psi_{xy} = \dfrac{1}{2}\left(\dfrac{\partial u}{\partial y} + \dfrac{\partial v}{\partial x}\right) \\ \psi_y = \dfrac{\partial v}{\partial y}, \psi_{yz} = \dfrac{1}{2}\left(\dfrac{\partial v}{\partial z} + \dfrac{\partial w}{\partial y}\right) \\ \psi_z = \dfrac{\partial w}{\partial z}, \psi_{zx} = \dfrac{1}{2}\left(\dfrac{\partial w}{\partial x} + \dfrac{\partial u}{\partial z}\right) \end{cases} \quad (2)$$

where ψ_x, ψ_y and ψ_z represent the normal strains in the x, y and z directions, respectively; u, v and w are the displacements in the corresponding directions; ψ_{xy}, ψ_{yz} and ψ_{zx} represent the shear strains in the respective directions.

The physical equation between stress and strain:

$$\begin{cases} \psi_x = \dfrac{\sigma_x - \mu(\sigma_y + \sigma_z)}{E} \\ \psi_y = \dfrac{\sigma_y - \mu(\sigma_z + \sigma_x)}{E} \\ \psi_z = \dfrac{\sigma_z - \mu(\sigma_x + \sigma_y)}{E} \end{cases} \quad (3)$$

where E is the modulus of elasticity, and μ is the Poisson's ratio (Table 2).

2.3 Impact of assembly pressure on the physical properties of GDL

It is assumed that all components except the GDL in a PEMFC remain rigid. Due to the structure of flow channels and ribs in the BP, the deformation of the GDL is non-uniform. Along the x-axis of the fuel cell, the thickness of the GDL under the channels and ribs varies, and this difference becomes more obvious under higher pressures. Moreover, the physical properties of the GDL change with its compression deformation. For instance, properties such as porosity,[29] permeability,[30] contact resistance,[31] and conductivity[30] are all affected by the compression deformation of the GDL. The corresponding relation equations can be found from these literatures.

From our previous research, it is known that under the assembly load, the flow channels and the ribs exert distinctly

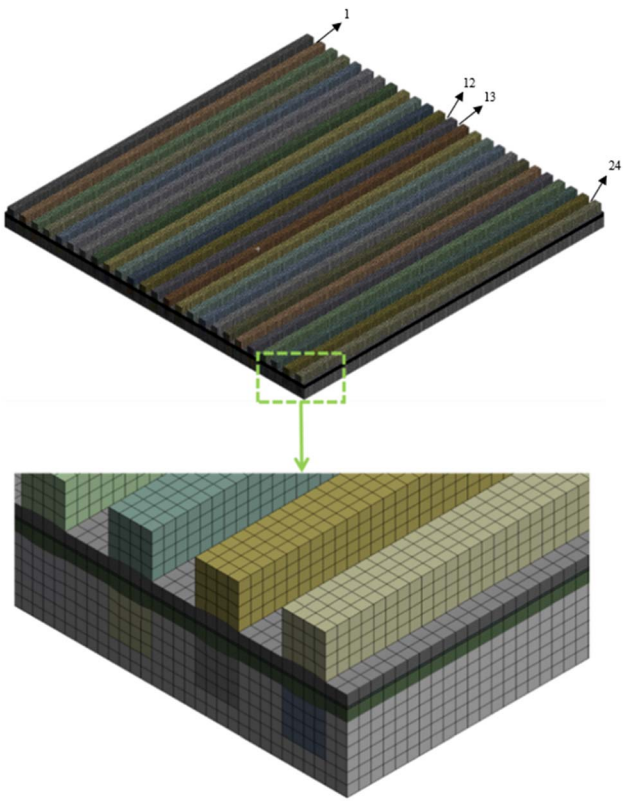

Fig. 2 Mesh diagram of the PEMFC under 0.5 MPa.

Table 3 Basic model parameters and operating conditions

Parameters	Values
Operating temperature (K)	353.15
Operating pressure (Pa)	101 325
Anode stoichiometric ratio	1.5
Cathode stoichiometric ratio	2
Anode gas relative humidity	80%
Cathode gas relative humidity	100%
Open circuit voltage[34] (V)	1.1
Faraday constant (C mol^{-1})	96 485

different forces on the GDL beneath them, creating different stresses and strains. Under these forces, the porous GDL and CL under the ribs undergo microstructural changes, such as a decrease in porosity and the transformation of large pores into smaller pores, while there is virtually no change in the middle of the flow channels. However, at the junction of the ribs and flow channels, a significant nonlinear transition occurs. These microstructural changes lead to complex variations in physical properties such as thermal conductivity, electrical conductivity, permeability, and diffusion coefficients of components, thereby affecting fluid flow and mass transfer. These research findings can be referenced from our previous study.[26]

3. Computational fluid dynamics model for transport processes within a fuel cell

3.1 Basic assumptions

When the PEMFC operates, its internal transport processes is extremely complex, involving multi-component, multiphase, and multidimensional flow phenomena, accompanied by the transfer of heat and mass, as well as electrochemical reactions. These complicated phenomena primarily occur in the very thin porous structures of the GDL, CL, and PEM.[32,33] The further research is needed to deeply consider the specific impact of compression deformation on the above transport processes caused by the fuel cells assembly.

In order to construct a simplified mathematical model of the PEMFC, the following basic assumptions were made:

(1) The fuel cell is in a stable operating state;

(2) Other materials are isotropic except the GDL;

(3) The deformation of GDL under different assembly pressures is considered, the rest of the PEMFC components maintain their shape and size;

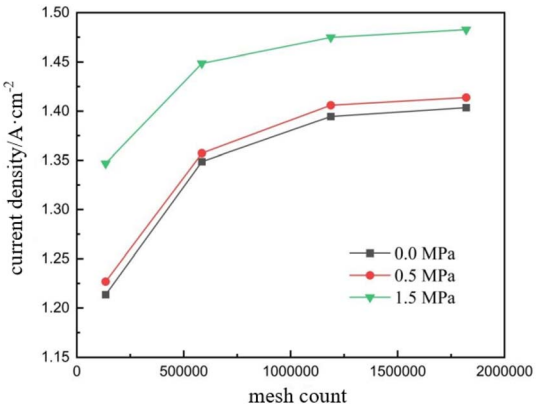

Fig. 3 Mesh independence verification.

(4) All gaseous species are treated as ideal gases, and the fluid flow is taken as laminar for the low Reynolds numbers.

3.2 Basic governing equations

Mass conservation equation:

$$\frac{\partial(\varepsilon\rho)}{\partial t} + \nabla\cdot(\varepsilon\rho\boldsymbol{u}) = S_{\mathrm{m}} \tag{4}$$

where ε represents the porosity of the porous medium; ρ is the density; $\boldsymbol{u}$ is the velocity vector. ∇ is the operator; S_{m} is the mass source term.

Momentum conservation equation:

$$\frac{\partial(\varepsilon\rho\boldsymbol{u})}{\partial t} + \nabla\cdot(\varepsilon\rho\boldsymbol{u}\boldsymbol{u}) = -\varepsilon\nabla p + \nabla\cdot(\varepsilon\mu\nabla\boldsymbol{u}) + S_{\boldsymbol{u}} \tag{5}$$

where p represents the fluid pressure; S_{m} is the momentum source term.

Energy conservation equation:

$$\frac{\partial(\varepsilon\rho c_{\mathrm{p}}T)}{\partial t} + \nabla\cdot(\varepsilon\rho c_{\mathrm{p}}\boldsymbol{u}T) = \nabla\cdot(\lambda^{\mathrm{eff}}\nabla T) + S_{\mathrm{Q}} \tag{6}$$

where C_{p} represents the specific heat capacity of the fluid; T is the temperature; λ^{eff} is the effective thermal conductivity; S_{Q} is the energy source term.[18]

Species conservation equation

$$\frac{\partial(\varepsilon c_{\mathrm{i}})}{\partial t} + \nabla\cdot(\varepsilon\boldsymbol{u}c_{\mathrm{i}}) = \nabla\cdot(D_{\mathrm{i}}^{\mathrm{eff}}\nabla c_{\mathrm{i}}) + S_{\mathrm{i}} \tag{7}$$

where c_{i} represents the concentration of the component; $D_{\mathrm{i}}^{\mathrm{eff}}$ is the effective diffusion coefficient for the component; S_{i} is the source term for the component.

Liquid water transport equation

Table 4 Material properties of PEMFC components

Parameters	PEM	GDL	CL	End plate
Electrical conductivity[24] (S m^{-1})	9.825	300	300	20 000
Thermal conductivity (W m^{-1} K^{-1})	0.95	1	1	20
Specific heat capacity (J kg^{-1} K^{-1})	833	568	3300	1580
Thermal expansion coefficient[27] (K)	1.23×10^{-4}	2.5×10^{-6}	3.7×10^{-5}	0.9×10^{-6}

$$r_w = \frac{\partial(\varepsilon\rho_l z)}{\partial t} + \nabla\cdot(\rho_l \boldsymbol{u}_l z) \quad (8)$$

where ρ_l represents the density of liquid water; z is the liquid saturation; $\boldsymbol{u}_l$ is the liquid velocity.

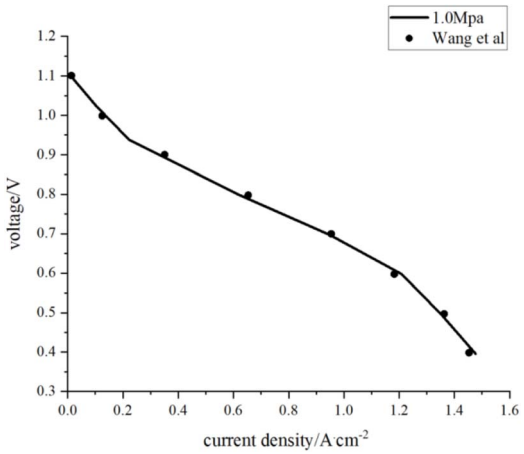

Fig. 4 Comparison between the simulated and experimental performance.

Charge conservation equation

$$\nabla\cdot(\gamma_j^{\text{eff}}\nabla\phi_j) = S_{\phi_j} \quad (9)$$

where γ represents the electrical conductivity; ϕ is the electric potential; j refers to the solid and membrane phases (s or m); eff stands for effective; S_{ϕ_j} is the charge source term. The expressions for the source terms are consistent with our previous research.[26]

3.3 Computational methods and model parameters

The deformed fuel cells model obtained from the previous FEA was meshed as shown in Fig. 2 and imported into FLUENT for fuel cells CFD simulation calculations. The SIMPLEC algorithm was used to solve the coupled equations for velocity and pressure. The method using a given working voltage to obtain the current density was employed to obtain the fuel cells performance curve. The open circuit voltage was set as 1.1 V, with working voltages ranging from 1.0 V to 0.3 V, in increments of 0.1 V. The parameters and operating conditions of the PEMFC used in the simulation are listed in Tables 3 and 4.

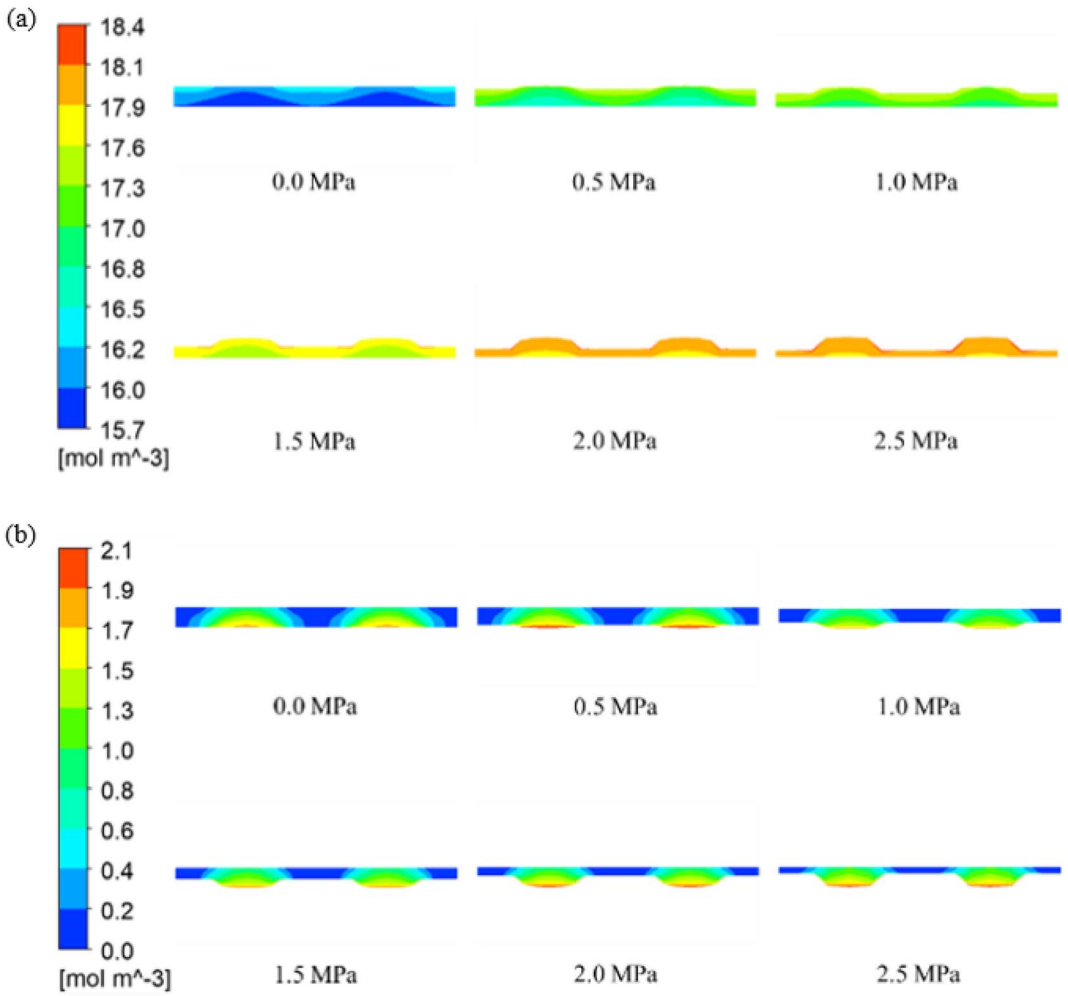

Fig. 5 Distribution at the *xy* cross-section in the non-uniformly deformed GDL under the 12th and 13th channels: (a) hydrogen; (b) oxygen.

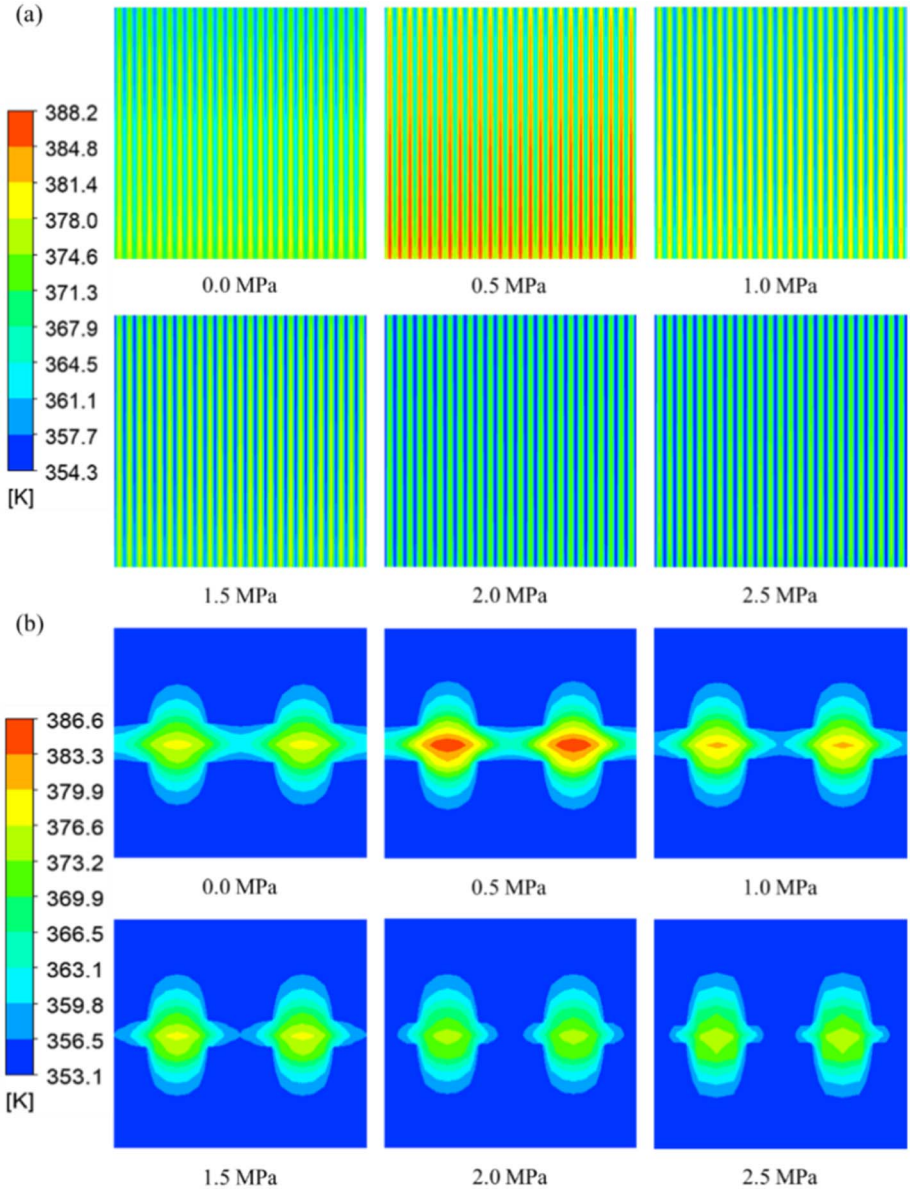

Fig. 6 Temperature distribution: (a) the interface of PEM and CL; (b) the *xy* cross-section of the fuel cell under the 12th and 13th channels.

3.4 Mesh independence verification

In order to balance the accuracy and time of calculation, the grid independence of compressed model was verified, using mesh sizes of 135 000, 585 000, 1 188 000, and 1 821 000. For the compressed single-channel model under pressures of 0.0, 0.5, and 1.5 MPa, respectively, the current densities at the voltage of 0.4 V were compared. As illustrated in Fig. 3, the value increased with the mesh count. The variation in current density was less than 1% with 188 000 grids, which was therefore selected for the later simulations.

4. Results and analysis

The simulation results of PEMFC considering non-uniformly deformation obtained at 1.0 MPa was compared with the experimental data from ref. 35. The results showed good agreement, indicating the reliability of the mathematical model and numerical simulation (Fig. 4).

4.1 Mass transfer distribution

The influence of non-uniform deformation obtained at various assembly pressures on the mass transfer in each electrode and also the compressed GDL is studied. Fig. 5 shows the reactants concentration distributions at anode and cathode ($z = 25$ mm cross-section), respectively. As the degree of compression increased, the average hydrogen molar concentration in the anode increased from 16.11 to 18.1 mol m^{-3}, and the average oxygen value in the cathode increased from 0.54 to 1 mol m^{-3}. It was revealed that the gas concentration under the rib region is significantly lower than that under the flow channel. In

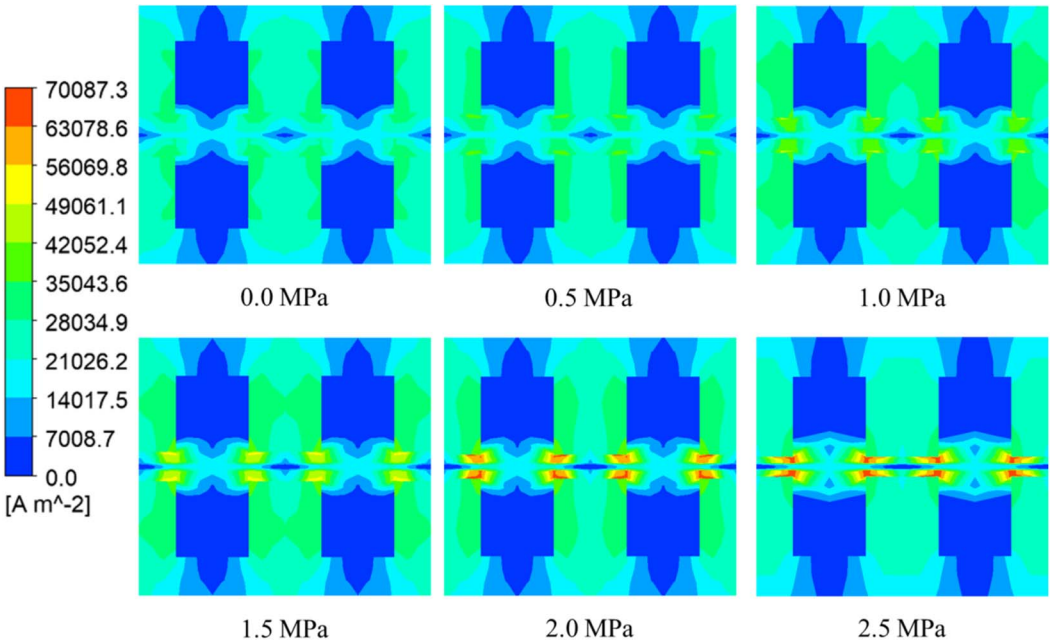

Fig. 7 Distribution of current density under the 12th and 13th channels (at the cross-sections at $z = 25$ mm).

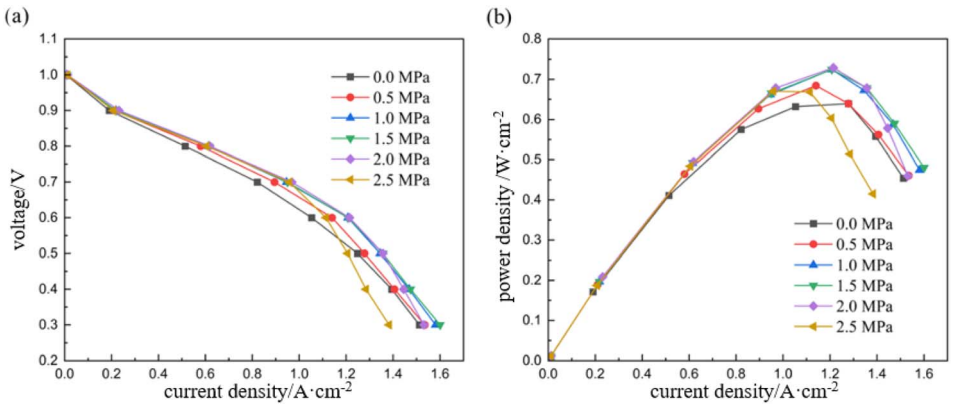

Fig. 8 Performance curves under different deformation conditions: (a) the voltage–current density curves; (b) the power density-current density curves.

contrast, the flow channel region had less deformation, resulting in lower gas transfer resistance. Additionally, because of higher diffusion coefficient, the increase of hydrogen concentration in the anode is lower than that of oxygen in the cathode. Moderate deformation could optimize the gas distribution, enhancing the transport of reactant gases to the catalyst layer and thereby improving cell performance.

4.2 Temperature distribution

Fig. 6 shows the temperature distribution at the PEM-CL interface and on the *xy*-plane at $z = 25$ mm within the cell. It can be seen from the figure that the peak temperature at the PEM-CL interface initially increases and then decreases with pressure. The highest temperature is reached at 0.5 MPa, peaking at 386.6 K, and then decreases to 375.9 K at 2.5 MPa. The peak temperature has a nonlinear relationship with pressure; at 0.5 MPa, due to active electrochemical reactions but insufficient heat dissipation, the temperature accumulates to the highest. While this condition can enhance performance in the short term, prolonged high temperatures will reduce fuel cell life. From 1.0 to 2.0 MPa, as pressure increases, the gas flow rate accelerates, which benefits heat dissipation and helps control the temperature. At 2.5 MPa, the rate of chemical reactions decreases, heat production is reduced, and the temperature subsequently drops. Fig. 6(b) reveals that the temperature is always highest in the MEA area, due to the main chemical reactions occurring there.

4.3 Current density distribution

The distribution of current density in the fuel cell at cross-section ($z = 25$ mm) after compression is shown in Fig. 7. It can be seen from the figure that the peak current density is

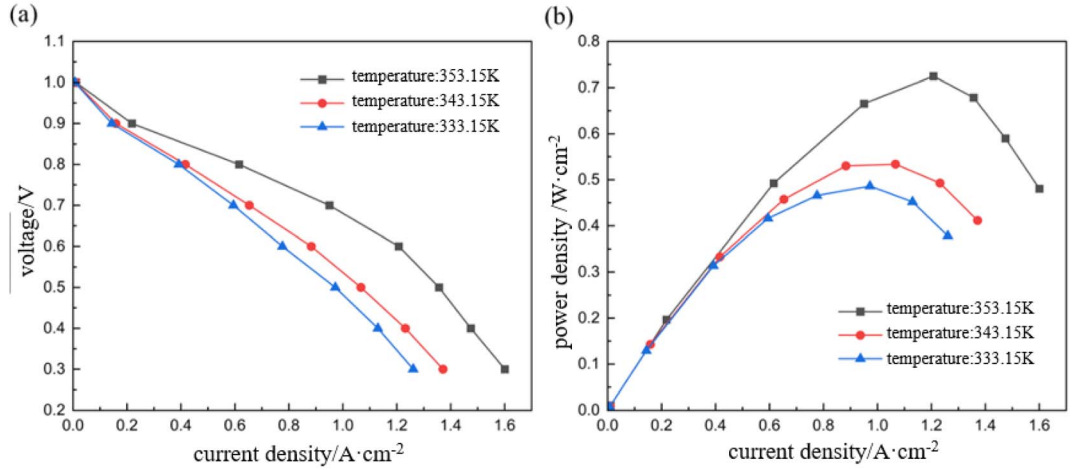

Fig. 9 Performance curves at different operating temperatures under pressure 1.5 MPa: (a) the voltage–current density curve; (b) the power density–current density curve.

found at the GDL beneath the joint of the channel and the rib, whose value increased with the deformation degree. As electrons flowed from the shortest distance through the rib to the external circuit, a significant number of electrons accumulated at the intersection of the channel and the rib, resulting in higher current densities. The non-uniformly distributed current density may lead to localized overheating, affecting fuel cell performance and lifespan.

4.4 Performance curves

Fig. 8 shows the output performance of the fuel cell under different compression conditions. The assemble pressure mostly affected the mass transfer at high current density. The highest current density and power density were achieved under proper assembly. As higher pressures contributed more serious non-uniformly deformation, the porosity and permeability of GDL and the contact resistance between the GDL and BP were reduced. Therefore, an optimal compression range that balanced mass transfer conditions and contact resistance could optimize cell performances. So the medium pressure 1.5 MPa is the optimal assemble pressure.

4.5 Influence of operating temperature, gas relative humidity and stoichiometric ratio on polarization curves under optimal assembly pressure 1.5 MPa

Fig. 9 shows the fuel cell performance curves at three different operating temperatures 353.15 K, 343.15 K, and 333.15 K under optimal assembly pressure 1.5 MPa. As the temperature decreases, the current density also gradually decreases, with values of 1.6 A cm^{-2}, 1.37 A cm^{-2}, and 1.26 A cm^{-2} respectively. The peak power densities are 0.725 W cm^{-2}, 0.534 W cm^{-2}, and 0.486 W cm^{-2}. The reductions are approximately 16.8% to 27% and 35.8% to 49.2% at 343.15 K and 333.15 K, respectively, compared to 353.15 K. This indicates that within the temperature range of 333.15 K to 353.15 K, the operating temperature significantly impacts cell performance. A decrease in operating

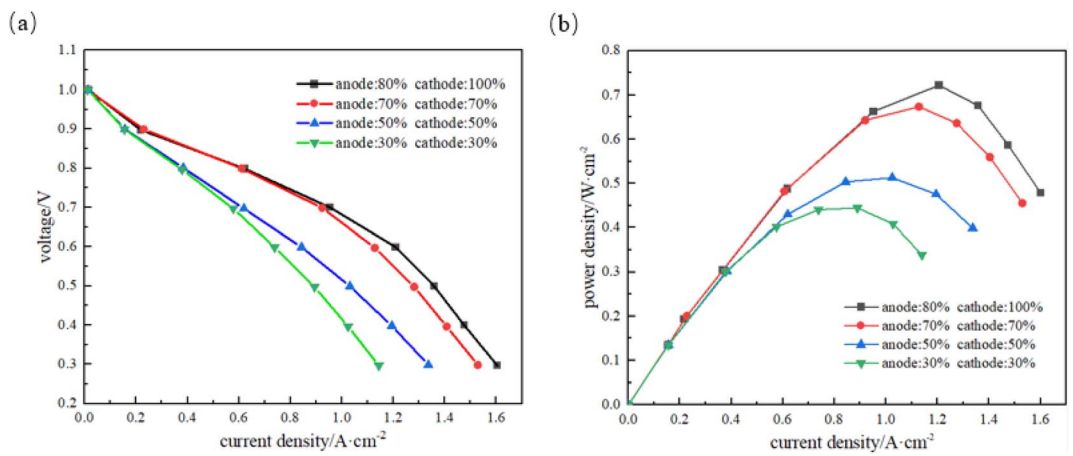

Fig. 10 Performance curves under different gas relative humidity: (a) the voltage–current density curve; (b) the power density–current density curve.

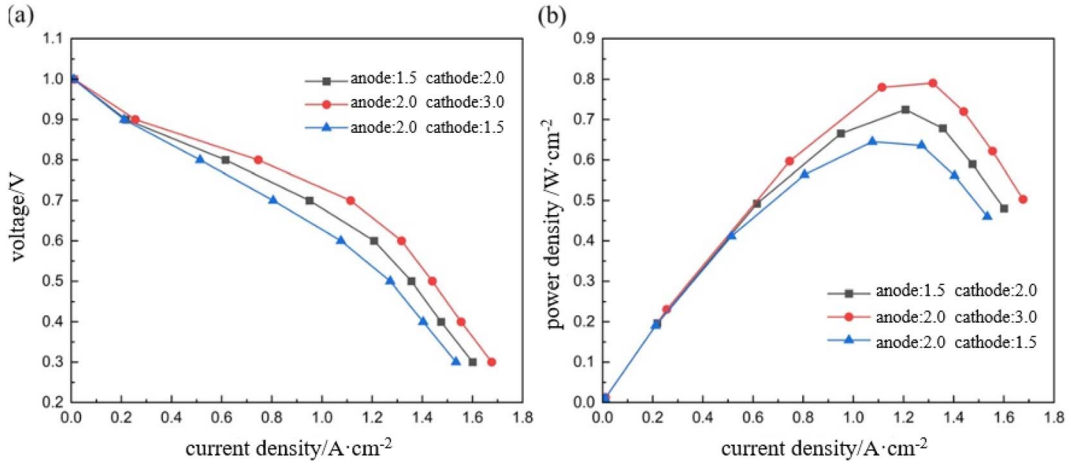

Fig. 11 Performance curves under different stoichiometries: (a) the voltage–current density curve; (b) the power density–current density curve.

temperature leads to a significant reduction in current and power density, which is consistent with the conclusions of most studies. The main reason is that higher temperature can cause faster reaction and higher exchange current density.

To investigate the effects of inlet gas relative humidity on performance in PEMFCs, four sets of relative humidity combination were used: anode 80% and cathode 100%, anode 70% and cathode 70%, anode 50% and cathode 50%, and anode 30% and cathode 30%. Fig. 10 shows the cell performance curves at different gas relative humidity under optimal assembly pressure 1.5 MPa. It can be observed that the highest current density (1.6 A cm^{-2}) and power density (0.725 W cm^{-2}) occur at an anode humidity of 80% and a cathode humidity of 100%. As the humidity decreases from anode 80% and cathode 100% to both anode and cathode at 30%, the current density and power density decrease by 40.4% and 62.6%, respectively. This indicates that lower humidity significantly reduces cell performance, primarily due to a decrease in the water content of the proton exchange membrane, which increases its membrane resistance, thereby reducing current density and power density.

In order to study the effects of stoichiometry on the performance of PEMFCs, a comparative analysis of three combinations was conducted: anode 1.5 and cathode 2, anode 2 and cathode 1.5, and anode 2 and cathode 3. The polarization curves of fuel cells under different stoichiometric ratios combination under optimal assembly pressure 1.5 MPa are shown in Fig. 11. The maximum current densities and power densities increased with the ratio. It was also indicated that better performances are obtained with higher reactant ratio at cathode. The bigger stoichiometric ratios can remove liquid water and transfer reactants to the CL under rib more effectively, and then obtain better performance.

5. Summary

In this paper, the influence of different assembly pressure (0–2.5 MPa) on the geometrical deformation and performance of PEMFC was studied using ANSYS static analysis. Using CFD technology and FLUENT software, a three-dimensional two-phase flow PEMFC model was constructed and solved, and the influence of assembly pressure on mass transfer and performance of PEMFC was deeply analyzed.

(1) Due to non-uniform deformation, the porosity and permeability of GDL decrease significantly, especially the region under rib, which is not conducive to chemical species, resulting in water retention and decreased gas concentration. At the same time, GDL compression reduces the contact resistance and increases the conductivity, thereby reducing the total resistance and helping to suppress the thermal effect of the fuel cell.

(2) The ideal range of assembly pressure for PEMFCs is between 1.0 to 2.0 MPa. At an assembly pressure of 1.5 MPa and a voltage of 0.3 V, the cell achieves a maximum current density of about 1.6 A cm^{-2}; while at an assembly pressure of 2.0 MPa and a voltage of 0.6 V, the maximum power density of the cell is 0.73 W cm^{-2}. For low voltage conditions of 0.3 V and 0.4 V, an assembly pressure of 1.0–1.5 MPa is suitable; whereas for voltage conditions of 0.5–0.7 V, an assembly pressure of 1.0–2.0 MPa is more appropriate, significantly enhancing cell performance.

(3) At an optimal assembly pressure of 1.5 MPa, the cell exhibits the best overall performance at a temperature of 353.15 K, with an anode at 80% and a cathode at 100% relative humidity, and a stoichiometric ratio of 2 at the anode and 3 at the cathode.

Data availability

All the data supporting this article have been included in the research article.

Author contributions

Wang Zheng: investigations, writing – original draft, software, formal analysis. Yuzhen Xia: investigations, methodology, writing – review & editing, supervision. Hangwei Lei: investigations, writing-original draft, formal analysis. Haoze Wang:

investigations, writing – original draft, software. Guilin Hu: investigations, conceptualization, writing – review & editing, supervision.

Conflicts of interest

There are no conflicts to declare.

Acknowledgements

This study was funded by Zhejiang Provincial Outstanding Youth Science Foundation (R1100065), Basic Research Fund Project of Zhejiang University of Science and Technology (2025QN075) and Research Project of Zhejiang Provincial Department of Education (Y202455204).

References

1 R. O'hayre, S. Cha, W. Colella, *et al. Fuel Cell Fundamentals*, John Wiley & Sons, 2016.
2 Q. Xiu, K. Lum, H. J. Poh, *et al.*, Optimization of assembly clamping pressure on performance of proton-exchange membrane fuel cells, *J. Power Sources*, 2010, **195**, 62–68.
3 C. Carral and P. Mélé, A numerical analysis of PEMFC stack assembly through a 3D finite element model, *Int. J. Hydrogen Energy*, 2014, **39**(9), 4516–4530.
4 A. Uzundurukan, M. Bilgili and Y. Devrim, Examination of compression effects on PEMFC performance by numerical and experimental analyses, *Int. J. Hydrogen Energy*, 2020, **45**(60), 35085–35096.
5 Q. Wang, F. Tang, B. Li, *et al.*, Investigation of the thermal responses under gas channel and land inside proton exchange membrane fuel cell with assembly pressure, *Appl. Energy*, 2022, **308**, 118377.
6 J. Chen, W. Gao, T. Ning, *et al.*, Effect of GDL compression on PEMFC performance: A comprehensive cross-scale study, *Chem. Eng. J.*, 2025, **503**, 158542.
7 J. Wang, J. Yuan and B. Sunden, On electric resistance effects of non-homogeneous GDL deformation in a PEM fuel cell, *Int. J. Hydrogen Energy*, 2017, **42**(47), 28537–28548.
8 P. Lin, P. Zhou and C. Wu, A high efficient assembly technique for large PEMFC stacks. Part I, *J. Power Sources*, 2009, **194**, 381–390.
9 P. Lin, P. Zhou and C. Wu, A high efficient assembly technique for large PEMFC stacks Part II, *J. Power Sources*, 2010, **195**, 1383–1392.
10 Z. Zhang, J. Zhang, S. Hu, *et al.*, An effective equivalent stiffness model combined with equivalent beam model to predict the contact pressure distribution for a large PEM fuel cell stack, *Int. J. Hydrogen Energy*, 2023, **48**(30), 11431–11441.
11 X. Yan, C. Lin, Z. Zheng, *et al.*, Effect of clamping pressure on liquid-cooled PEMFC stack performance considering inhomogeneous gas diffusion layer compression, *Appl. Energy*, 2020, **258**, 114073.
12 L. Yang, Z. Sun, G. Zhang, *et al.*, Unmasking the reactants inhomogeneity in gas diffusion layer and the performances of PEMFC induced by assembly pressure, *Heliyon*, 2024, **10**(12), e32501.
13 Y. Zhou, K. Jiao, Q. Du, *et al.*, Gas diffusion layer deformation and its effect on the transport characteristics and performance of proton exchange membrane fuel cell, *Int. J. Hydrogen Energy*, 2013, **38**(29), 12891–12903.
14 P. Gigos, Y. Faydi and Y. Meyer, Mechanical characterization and analytical modeling of gas diffusion layers under cyclic compression, *Int. J. Hydrogen Energy*, 2015, **40**(17), 5958–5965.
15 Y. Chen, J. Zhao, C. Jin, *et al.*, Effect of clamping compression on the mechanical performance of a carbon paper gas diffusion layer in polymer electrolyte membrane fuel cells, *Membranes*, 2022, **12**(7), 645.
16 M. Espinoza, M. Andersson, J. Yuan, *et al.*, Compress effects on porosity, gas-phase tortuosity and gas permeability in a simulated PEM gas diffusion layer, *Int. J. Energy Res.*, 2015, **39**(11), 1528–1536.
17 N. Kulkarni, J. Cho, R. Jervis, *et al.*, The effect of non-uniform compression on the performance of polymer electrolyte fuel cells, *J. Power Sources*, 2022, **521**, 230973.
18 J. Wang, J. Yuan and B. Sundén, On electric resistance effects of non-homogeneous GDL deformation in a PEM fuel cell, *Int. J. Hydrogen Energy*, 2017, (47), 28537–28548.
19 M. Zheng, H. Liang, W. Bu, *et al.*, Design and performance optimization of a lattice based radial flow field in proton exchange membrane fuel cells, *RSC Adv.*, 2024, **14**, 32542.
20 P. Chi, S. Chan, F. Weng, *et al.*, On the effects of non-uniform property distribution due to compression in the gas diffusion layer of a PEMFC, *Int. J. Hydrogen Energy*, 2010, **35**(7), 2936–2948.
21 P. Chippar, O. Kyeongmin, K. Kang, *et al.*, A numerical investigation of the effects of GDL compression and intrusion in polymer electrolyte fuel cells (PEFCs), *Int. J. Hydrogen Energy*, 2012, **37**(7), 6326–6338.
22 Z. Su, C. Liu, H. Chang, *et al.*, A numerical investigation of the effects of compression force on PEM fuel cell performance, *J. Power Sources*, 2008, **183**(1), 182–192.
23 H. Zhang, M. Rahman, F. Mojica, *et al.*, A comprehensive two-phase proton exchange membrane fuel cell model coupled with anisotropic properties and mechanical deformation of the gas diffusion layer, *Electrochim. Acta*, 2021, **382**, 138273.
24 D. Jiao, K. Jiao, S. Zhong, *et al.*, Investigations on heat and mass transfer in gas diffusion layers of PEMFC with a gas–liquid-solid coupled model, *Appl. Energy*, 2022, **316**, 118996.
25 Z. Dong, Y. Liu, Y. Qin, *et al.*, Coupled FEM and CFD Modeling of Structure Deformation and Performance of PEMFC Considering the Effects of Membrane Water Content, *Energies*, 2022, **15**(15), 5319.
26 H. Lei, Y. Xia and G. Hu, Effects of inhomogeneous gas diffusion layer properties on the transportation phenomenon and performances of proton-exchange membrane fuel cells, *ACS Omega*, 2024, **9**(8), 9383–9395.
27 G. Hu, C. Ji, Y. Xia, *et al.*, Assembly mechanics and its effect on performance of proton exchange membrane fuel cell, *Int. J. Electrochem. Sci.*, 2019, **14**(2), 1358–1371.

28 W. Li, W. Yang, W. Zhang, *et al.*, Three-dimensional modeling of a PEMFC with serpentine flow field incorporating the impacts of electrode inhomogeneous compression deformation, *Int. J. Hydrogen Energy*, 2019, **44**(39), 22194–22209.
29 K. Jiao, J. Park and X. Li, Experimental investigations on liquid water removal from the gas diffusion layer by reactant flow in a PEM fuel cell, *Appl. Energy*, 2010, **87**(9), 2770–2777.
30 M. Tomadakis and T. I. Robertson, Viscous permeability of random fiber structures: comparison of electrical and diffusional estimates with experimental and analytical results, *J. Compos. Mater.*, 2005, **39**(2), 163–188.
31 V. Mishra, F. Yang and R. Pitchumani, Measurement and prediction of electrical contact resistance between gas diffusion layers and bipolar plate for applications to PEM fuel cells, *J. Fuel Cell Sci. Technol.*, 2004, **1**(1), 2–9.
32 J. Larminie and A. Dicks, *Fuel Cell Systems Explained*, J. Wiley, Chichester, UK, 2003.
33 J. Zhang, *PEM Fuel Cell Electrocatalysts and Catalyst Layers: Fundamentals and Applications*, Springer, London, 2008.
34 K. Oh, P. Chippar and H. Ju, Numerical study of thermal stresses in high-temperature proton exchange membrane fuel cell (HT-PEMFC), *Int. J. Hydrogen Energy*, 2014, **39**(6), 2785–2794.
35 Y. Wang, S. Wang, S. Liu, *et al.*, Optimization of reactants relative humidity for high performance of polymer electrolyte membrane fuel cells with co-flow and counter-flow configurations, *Energy Convers. Manage.*, 2020, **205**, 112369.